Flowfield Characteristics and Performance Limitations of Quasi-Steady Magnetoplasmadynamic Accelerators

M. J. Boyle,* K. E. Clark,† and R. G. Jahn‡
Princeton University, Princeton, N. J.

Measurements of terminal voltage, exhaust velocity, current and potential distributions in a quasi-steady magnetoplasmadynamic (MPD) arc operating over a range of currents from 3 to 25 kA countervene previous indications of basic limitations on MPD performance. Terminal voltage fluctuations, previously used as an indicator of a unique limiting value of the parameter $J^2/\dot{m}$ (current squared over mass flow), are shown to be related to cathode surface area rather than to interelectrode plasma phenomena. With improved electrodes and insulators, satisfactory arc operation at specific impulses somewhat beyond previously proposed limits has been demonstrated, and the significant thrust producing mechanisms in such arcs have been identified.

Introduction

THE ultimate capabilities of MPD arcjets can only be established from detailed understanding of the plasma acceleration mechanisms and associated loss processes, or from very extensive empirical testing, neither of which are in hand, or readily attainable. In their absence, several attempts have been made to postulate fundamental limitations on the attainable performance of various MPD arcs on the basis of semiempirical models and restricted performance data.[1-6] The general validity of these proposed limitations, or the possible existence of others, is crucial to the eventual utility of MPD accelerators as space thrusters; hence, they merit more detailed analytical and experimental examination.

In principle, self-field MPD thruster performance should improve with increased power in the multimegawatt region, since thrust density and specific impulse are increasing functions of arc current. Specifically, since the self-field electromagnetic thrust T scales quadratically with arc current, it follows that the exhaust velocity u and the specific impulse I_s are proportional to the parameter $J^2/\dot{m}$

$$T=\dot{m}u=bJ^2 \tag{1}$$

$$I_s=u/g=T/\dot{m}g=(b/g)\,(J^2/\dot{m}) \tag{2}$$

where b is the self-field electromagnetic thrust coefficient derivable from an electromagnetic stress tensor,[7] and g is the standard acceleration of gravity. For a given mass flow rate, arcjet operation at higher currents should yield disproportionally higher performance. Furthermore, it has been demonstrated experimentally that the major fractional power loss in the accelerator, the anode heat transfer, scales inversely with arc power,[8] implying that thrust efficiency should correspondingly increase with input power. However, certain other observations have been interpreted to imply that quasi-steady thruster performance may be inherently limited because of an unavoidable coupling between the arc current and the accelerated mass flow rate. As arc currents are increased for given propellant flow rates, a point is reached above which various undesirable effects occur, such as insulator and electrode ablation, mass recirculation, and terminal voltage fluctuations. The onset of these effects is taken as a manifestation of a fundamental upper limit on arc current for a given flow rate, with a corresponding maximum attainable specific impulse.

For example, Malliaris et al.[9] observed, for a given propellant and mass flow rate, a certain arc current J^* above which the terminal voltage became erratic. The onset of this erratic behavior scaled such that the parameter $(J^*)^2/\dot{m}$ remained constant for a given propellant. This observation was rationalized analytically by a model which assumed that the discharge accelerates a net mass flow, not necessarily identical with the injected propellant flow rate, which just minimizes the power invested in the plasma stream. This minimum-power criterion yields limiting values for the exhaust velocity and specific impulse

$$I_c=u_c/g=(2e\phi_i/M_i)^{1/2}/g \tag{3}$$

which depend only on the propellant ionization potential ϕ_i and ion mass M_i. If only electromagnetic thrust mechanisms are significant, this transcribes via Eq. (2) into a critical value of the $J^2/\dot{m}$ parameter, which was found to be in good agreement with the experimental $(J^*)^2/\dot{m}$ for several different propellants. This model predicts a maximum specific impulse for argon of 890 sec, corresponding to an exhaust velocity of 8.7 km/sec. For helium, the value is 3500 sec; for xenon, 430 sec. Since the model presumes an energy equipartition between kinetic and ionization modes, the kinetic power efficiency of the accelerator is limited to 50%.

Despite the severe implications of this model, no further detailed experimental studies on its general validity appear to have been undertaken. Clearly, if the model is valid, one would like more detailed comprehension of the underlying arc phenomenology; if it is not, one needs a more serviceable criterion for charting arcjet performance. The key to either task lies in better understanding of the arcjet acceleration processes.

This paper describes a sequence of experimental studies of quasi-steady MPD arcjet operation in argon at or near the "critical" $J^2/\dot{m}$ condition which yield exhaust velocities in excess of the "limiting" value, and it presents a new acceleration model which accounts for this performance.

Experimental Facilities

The quasi-steady MPD accelerator and support systems used in the arc experiments are illustrated schematically in Fig. 1. The facilities consist of a mass-injection system, a pulse-forming network, the discharge chamber, a vacuum system, and assorted diagnostics. Argon propellant is sup-

Presented as Paper 75-414 at the AIAA 11th Electric Propulsion Conference, New Orleans, La., March 19-21, 1975; submitted May 1, 1975; revision received April 19, 1976. This work was supported by NASA Grant NGL 31-001-005.

Index categories: Electric and Advanced Space Propulsion; Plasma Dynamics and MHD.

*Graduate Student; presently Physicist, Lawrence Livermore Laboratories, Livermore, Calif.

†Research Engineer. Member AIAA.

‡Dean, School of Engineering and Applied Science. Fellow AIAA.

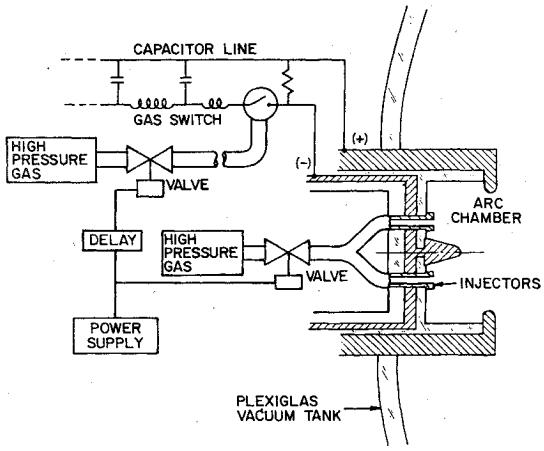

Fig. 1 Quasi-steady MPD arcjet apparatus.

plied to the discharge chamber through a fast-acting solenoid valve from a high-pressure reservoir. Choked orifices in the propellant feed lines control injected mass flow rates in a range between 1 and 32 g/sec.

Single, rectangular current pulses are generated by a 120-station LC ladder pulse-forming network.[10] This 160-kilojoule power supply has a total capacity of 3300 μfd and is capable of providing 1-msec pulses up to 26 kA when charged to 8 kV. An electronic delay circuit synchronizes the triggering of a gas switch in the pulse line with the time of stabilization of the injected propellant mass flow.

The cylindrical arc chamber is 12.7 cm in diam and 5.0 cm deep, and has a 1.9-cm diam thoriated tungsten cathode extending from the backplate, on the axis. Additional cathode dimensions and geometry are noted in the subsequent text where appropriate. The annular aluminum anode has an orifice diameter of 10.2 cm and an outer barrel diameter of 18.8 cm. The anode is electrically insulated from the cathode by a cylindrical Pyrex wall insert and a circular backplate. The insulator ablation discussed in the next section refers to the ablation of this plate. In addition to its function as an insulator, the backplate contains the injection orifices through which argon propellant is supplied to the discharge chamber. Changes in mass injection geometry refer to the use of backplates which vary the distribution of the injected propellant within the discharge chamber.

The accelerator exhausts the plasma into a Plexiglas vacuum tank 183 cm long and 92 cm i.d., evacuated by a 15.2-cm oil diffusion pump to 10^{-5} torr before each discharge. An electrically controlled probe carriage mounted inside the vacuum tank allows remote probing of the arc chamber and exhaust regions in three dimensions. Seven Plexiglas viewing ports mounted flush against the side and end of the vacuum tank permit unobstructed views of the entire discharge region for optical diagnostics.

During a nominal discharge sequence, a 1-msec, 15.3-kA current pulse establishes a diffuse, symmetric arc discharge between the accelerator electrodes, ionizing and accelerating an injected 6 g/sec argon gas pulse. Following a brief transient period, the electromagnetic and plasmadynamic flow-field patterns spatially stabilize for the remainder of the pulse. This latter period is referred to as the quasi-steady acceleration mode,[11] and is used throughout the program of experiments.

Removal of Insulator Ablation Effects

The proper evaluation of performance data for both steady and quasi-steady MPD arcjets has been hampered frequently by the perturbing influences of several extraneous phenomena. Ambient mass ingestion into the acceleration zones, insulator and electrode ablation, and the onset of voltage fluctuations all tend to distort the data, obscure the

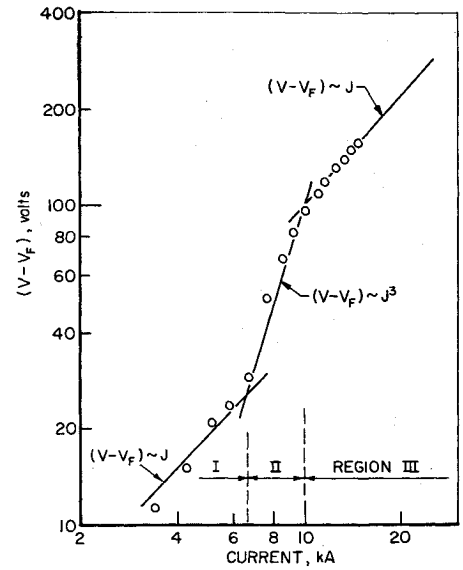

Fig. 2 *V-J* characteristic: $\dot{m}=6$ g/sec, 6-hole injection, Plexiglas backplate.

acceleration mechanisms, and otherwise prevent the evaluation of proper arcjet operation. For example, one quasi-steady arcjet study performed recently revealed a nonuniform spatial distribution of plasma species in the discharge resulting from Plexiglas insulator ablation.[12]

In the first experiments to be reported here, voltage-current characteristics and exhaust velocity profiles likewise suggest that both terminal arc voltages and final exhaust velocities can be influenced by insulator ablation.[13] Figure 2 shows the voltage-current characteristic for the arc operating with a six-hole Plexiglas insulator backplate and a total argon mass flow rate of 6 g/sec. In this case the argon propellant is injected axially into the discharge chamber through six 0.48-cm orifices symmetrically distributed about a 2.54-cm radius. The conical tungsten cathode is 2.54 cm in length and 1.9 cm in base diameter.

Electrode fall voltages are approximated by a linear extrapolation of the characteristic to its zero current value. The values so obtained are in good agreement with separate potential probe measurements taken in the vicinity of both electrodes. For the data in Fig. 2, a constant electrode fall of 25 V has been subtracted from all the terminal voltage data, to exhibit more clearly the arc column voltage dependence in the low current regime of the characteristic.

At the lowest currents, the self-electromagnetic forces are small, and the accelerator operates primarily in an electrothermal mode. In this range, the voltage may be expected to scale approximately linearly with the current.[14,15] The solid reference line of slope one in Fig. 2 delineates the current range over which electrothermal acceleration apparently prevails in this arc configuration (Region I).

At higher currents, electromagnetic acceleration predominates because of the dependence of the self-field force on the square of the current. In this high-current range, the arc column voltage is dominated by the motional EMF term of the generalized Ohm's law[7,14]

$$V_{II} \approx \int_c^a u \times B \cdot d\ell \tag{4}$$

where the self-induced magnetic field B scales linearly with arc current and the integration is along any convenient contour from the cathode to anode sheath surfaces. The electromagnetic domain is shown as Region II in Fig. 2 where the arc voltage scales as the cube of the current.

At yet higher currents, we encounter an unexpected, abrupt deviation from normal arcjet behavior, which is believed to be

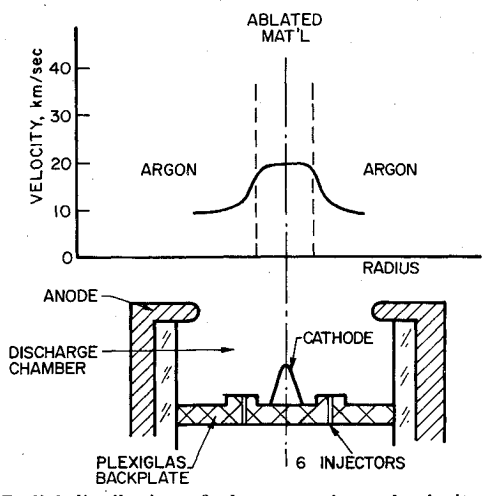

Fig. 3 Radial distribution of plasma species and velocity: $J = 15.3$ kA, $\dot{m} = 6$ g/sec.

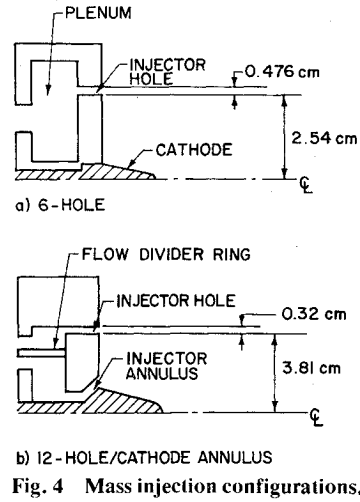

Fig. 4 Mass injection configurations.

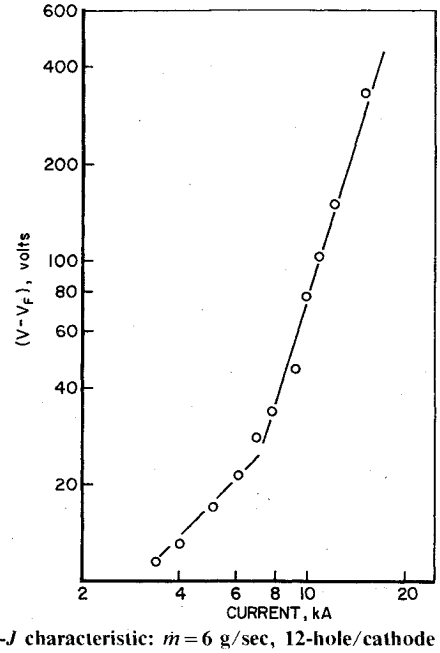

Fig. 5 V-J characteristic: $\dot{m} = 6$ g/sec, 12-hole/cathode annulus injection (50:50), boron nitride backplate.

associated with insulator ablation. Specifically, beyond 10 kA the characteristic reverts to a linear dependence of column voltage on current (Region III). Other quasi-steady thrusters purposely using ablated material as propellant have been found to ablate mass at a rate proportional to the square of the current.[16] For such thrusters, the self-field thrust relation of Eq. (1) implies that exhaust velocities should be independent of arc current; and indeed, velocity measurements in Region III of the characteristic indicate that the exhaust velocity is independent of current. It follows from relation (4), then, that ablation-dominated voltages should scale linearly with arc current. Region III of the characteristic apparently reflects such ablation-dominated operation of this arcjet.

A radial profile of exhaust velocity measured 2.5 cm downstream of the anode for this arc operating at 15.3 kA and 6 g/sec ($J^2/\dot{m} = 40$ kA^2 – sec/g) is shown in Fig. 3. The plasma velocities are measured using a time-of-flight double electric probe technique.[17] The profile consists of a central core region with an average plasma velocity of 21.0 km/sec and an outer annular region with an average velocity of 8.8 km/sec. When the radial species distribution determined earlier for this accelerator configuration[12] is superimposed upon this velocity profile, it is found that ionized dissociation products of Plexiglas ablation (carbon, oxygen, and hydrogen) are confined to the central core, while the injected argon propellant occupies the outer regions. It is therefore important to determine whether this velocity profile, particularly the highspeed central core, follows directly from the $j \times B$ body force distribution, or is more a consequence of the ablation of the particular insulator material employed within the arc chamber.

If the centerline Plexiglas plasma is treated as a monofluid with an effective ion mass equal to the weighted average atomic mass of the dissociated ablation products,

$$<m> = \frac{5m_c + 8m_h + 2m_o}{15} = 6.7 \quad \text{amu} \tag{5}$$

the ratio of the inverse square root of $<m>$ and the argon ion mass m_a corresponds within 2.5% to the experimentally measured velocity ratio:

$$<u>/u_a = (m_a/<m>)^{1/2} \tag{6}$$

This inverse square root mass dependence of species velocity has been observed previously by other investigators,[18] and we are thus led to suspect that the high centerline velocity is a consequence of the low average atomic mass of the centerline plasma, derived from the insulator ablation.

If the acceleration mechanisms and performance characteristics of the high power quasi-steady arc are to be properly evaluated, such effects of insulator ablation must either be accounted for or eliminated. For given levels of incident thermal flux, refractory insulating surfaces are less prone to ablate than Plexiglas surfaces. Accordingly, to reduce the effects of ablation, boron nitride was substituted for Plexiglas because of its higher thermal diffusivity and ablation temperature. Further, since visual and spectrographic data suggest that the insulator ablation is most severe about the base of the cathode where the inverse radial dependence of the local current density tends to maximize the thermal flux from the plasma to the insulating surface, an alternative injection geometry was designed to supply argon propellant directly to the cathode region and to eliminate insulator surface immediately adjacent to the cathode. In this annular cathode base mass injection configuration, shown in comparison to the previous 6-injector configuration in Fig. 4, the side of the cathode itself serves as one side of the annulus channel. In addition, twelve 0.32-cm-diam holes are symmetrically distributed about a 3.8-cm radius to assure a more uniform mass distribution in the vicinity of the anode. The flow division between inner annulus and outer holes is adjusted by varying the relative area of the choked orifices feeding the two independent plenums. In this

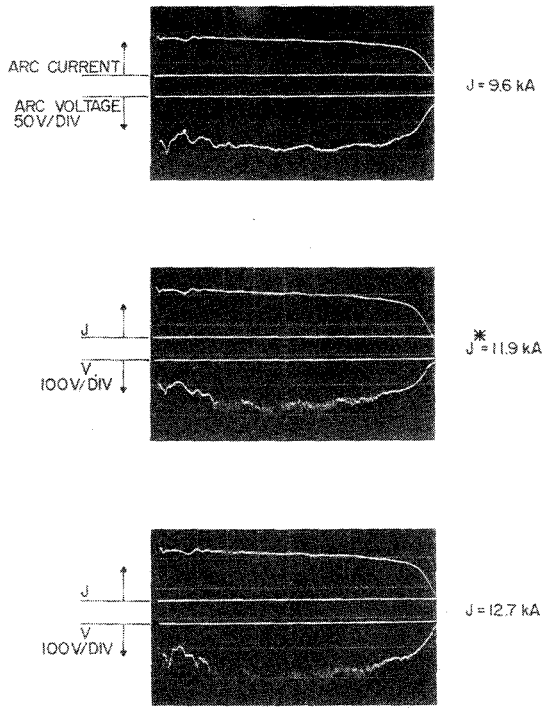

Fig. 6 Terminal voltage fluctuations: $\dot{m} = 6$ g/sec (50:50).

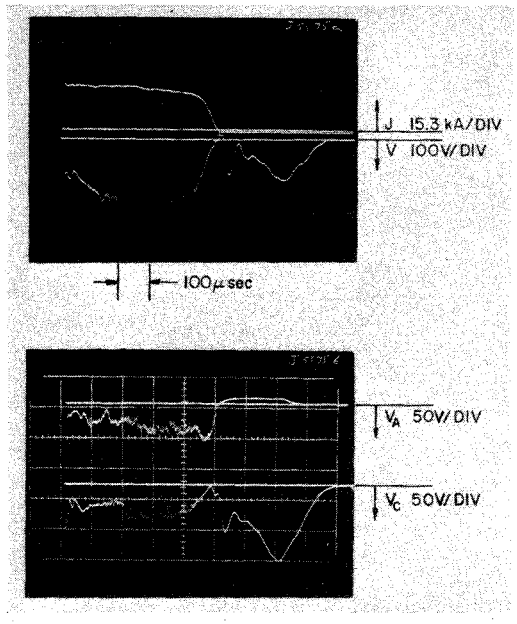

Fig. 7 Terminal voltage and floating potential signatures: $\dot{m} = 6$ g/sec (50:50).

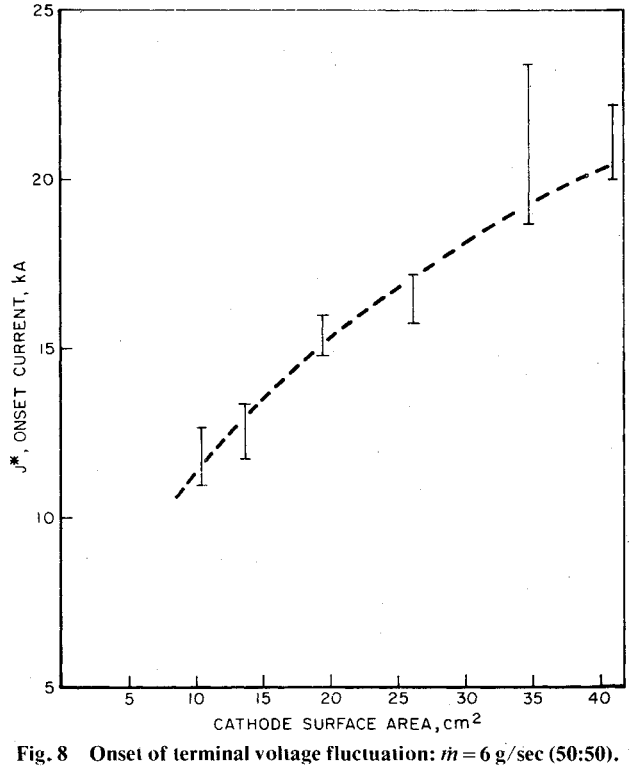

Fig. 8 Onset of terminal voltage fluctuation: $\dot{m} = 6$ g/sec (50:50).

manner the entire range of flow division between 100% inner flow, 0% outer flow (designated by 100:0), to 0% inner flow, 100% outer flow (0:100), may be spanned.

From a lengthy series of experiments, it was found that a 50:50 flow division between inner and outer injection orifices minimizes the arc voltage without reintroducing ablation-dominated exhaust velocities. At this condition, the azimuthal species structure of the discharge seen with the Plexiglas backplate is no longer evident, and the voltage-current characteristic for a total mass flow rate of 6 g/sec changes to that shown in Fig. 5. Regions I and II appear much the same as in the Plexiglas case, but now no transition to the ablation-dominated Region III occurs. Instead, the high current regime $J \geq 10$ kA continues to be characterized by a J^3 voltage dependence, typical of the normal electromagnetic mode, over the entire range tested. The centerline exhaust velocity 2.5 cm downstream of the anode orifice is now measured to be 9.0 km/sec at $J = 15.3$ kA, implying that the exhaust velocity pattern is no longer ablation-dominated. Thus, this combination of insulator material and mass injection geometry appears to provide an arcjet configuration whose plasma acceleration characteristics are independent of insulator ablation perturbations. Unless otherwise specified, the 50:50 flow division configuration using this boron nitride backplate was used throughout the experiments described hereafter.

Terminal Voltage Fluctuations

Even using refractory insulating materials and an optimum mass injection geometry, the arcjet still exhibits a limited range of satisfactory operation. For a given mass flow, there is a maximum current J^* beyond which the arc voltage becomes noisy, as illustrated in Fig. 6. For this mass flow of 6 g/sec, J^* is approximately 12 kA and the characteristic frequency of the fluctuation is several hundred kilocycles. For mass flow rates other than 6 g/sec, the fluctuations are found to appear at arc currents such that the parameter $(J^*)^2/\dot{m}$, has the same value.

Malliaris related the onset of such voltage fluctuations to a limitation on quasi-steady MPD arc operation, through a $J^2/\dot{m}$ parameter, which in his case took the value of 40 kA^2-sec/g for argon. In our experiments the onset value is 24 kA^2-sec/g. The two accelerators are similar in most details except for their cathode geometries, and one is thus tempted to look here to explain the disparity. That the onset of the voltage fluctuations might be associated with cathode phenomena is also suggested by spectral filter photographs of the cathode, which reveal different surface luminosity patterns for arc currents greater or less than J^*. Potential probes located close to the anode and cathode also indicate that the fluctuations in the terminal voltage signal arise from the vicinity of the cathode. Figure 7 compares the oscillogram signatures of the terminal voltage V with the potential drop between the cathode and a probe several millimeters off the cathode surface V_C, and with the potential several millimeters off the anode lip, measured with respect to the anode ground V_A, for

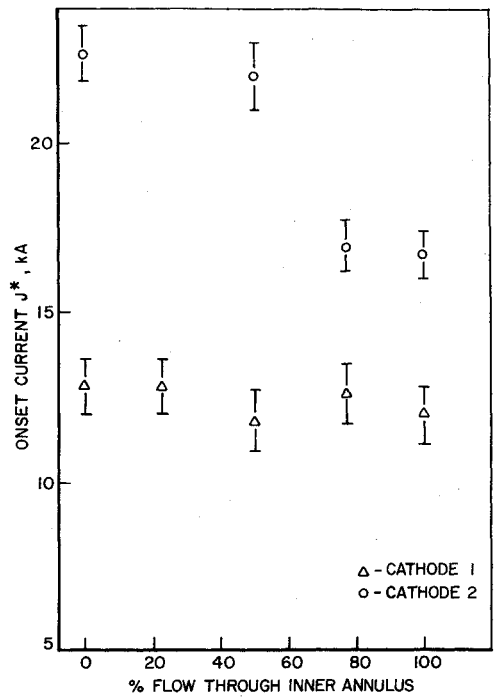

Fig. 9 Onset current vs flow division: $\dot{m} = 6$ g/sec.

an arc current greater than J^*. The cathode voltage signal clearly reproduces the onset time, frequency and amplitude of the terminal voltage fluctuation. Hence, the onset of erratic voltage seems related to processes occurring on, or in the vicinity of the cathode, rather than in the bulk of the plasma flow.

To investigate further the relation between noisy arcjet behavior and cathode surface area, the accelerator was operated with several different cathode geometries for a given mass flow and injection configuration. The current at which the arc voltage becomes noisy is presented as a function of cathode surface area in Fig. 8. J^* is seen to scale directly with the cathode area and to increase beyond the earlier limit of 15.3 kA. Experiments with even longer cathodes ($15 < L_c <$ 25 cm) confirm that J^* continues to increase over that range, but at a decreasing rate.[19] Regardless of the exact functional form of J^*, it now seems clear that the terminal voltage instability effect does not define a unique value of the $J^2/\dot{m}$ parameter as previously suggested.

The utility of the voltage fluctuation criterion is further compromised when the effect of mass injection geometry upon the steadiness of the terminal voltage signature is examined for fixed arc currents and cathode geometries. Division of the 6 g/sec injected argon was varied between 100% inner: 0% outer flow and 0% inner: 100% outer flow for two cathode geometries. A dependence of the onset current J^* upon flow division is found, which is itself dependent upon the relative area of the given cathode as shown in Fig. 9. For the smaller cathodes, typified by the Cathode 1 data in Fig. 9, J^* is insensitive to the manner in which the argon is distributed throughout the discharge chamber; the magnitude of J^* for all flow division is 12 kA, which is the value associated with the surface area of Cathode 1. However, for the larger cathodes, represented by the Cathode 2 data in Fig. 9, J^* exhibits an abrupt dependence upon the flow division. When less than 50% of the injected argon mass flow is delivered to the cathode region of the discharge chamber, the voltage becomes noisy at a J^* associated with the surface area of Cathode 2. The sudden drop to a lower onset current as less than 50% of the mass flow is injected towards the anode region suggests that a second process, possibly associated with anode starvation may be present. The sudden growth of fluctuating electric fields in the vicinity of the anode when insufficient charge carriers are supplied to that

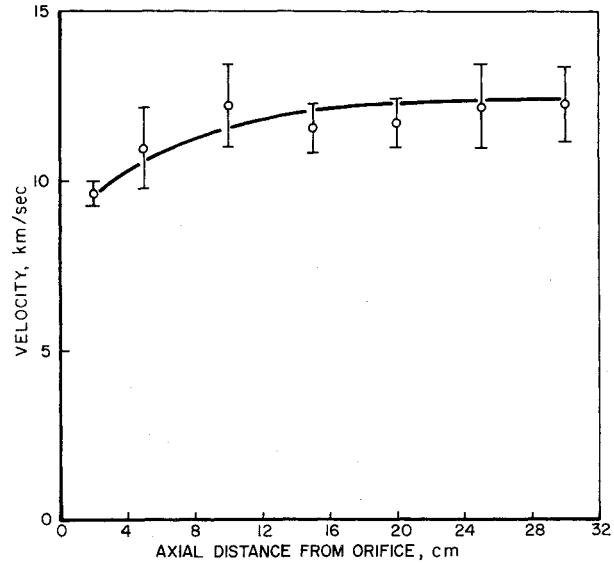

Fig. 10 Centerline axial velocity profile: $J = 15.3$ kA, $\dot{m} =$ g/sec (50:50).

region has been observed in other experiments.[2,20] In the case of the smaller cathodes, the cathode area effect apparently masks the onset of this second source of fluctuations. Whatever the cause of either fluctuation, it now appears that for sufficiently large cathodes and proper propellant distribution, nothing in the voltage behavior distinguishes the $J^2/\dot{m} = 40$ kA^2-sec/g operating condition as "critical" or fundamentally significant.

Quasi-Steady Plasma Acceleration Processes

With the insulator ablation, cathode surface area, and gas flow geometry properly under control, we may finally turn to systematic study of the acceleration processes of the MPD discharge itself, with continued emphasis on limiting conditions, real or imagined. In the series of experiments reported here, we concentrate on the Malliaris limiting condition, $J^2/\dot{m} = 40$ for argon. An accelerator with a boron nitride backplate, equal flow division between inner and outer injection orifices, and a 40-cm^2 cathode is operated at an arc current of 15.3 kA and a mass flow of 6 g/sec. The axial profile of exhaust velocity along the centerline measured by the time-of-flight probe technique is presented in Fig. 10. Velocity measurements within the discharge chamber are precluded by the lack of discernible ion density fluctuations required by the time-of-flight method, but the plasma is observed to leave the discharge chamber at a velocity less than 9.0 km/sec. This exhaust flow then continues to accelerate downstream for several anode orifice diameters, achieving a speed of 12.5 km/sec for argon.

To acquire some insight into the process by which the electrical input power is converted into directed motion of the propellant, maps of the current density and electric field patterns throughout the discharge were obtained. The current streamline pattern, obtained from magnetic probe data, is illustrated in Fig. 11, where each streamline is labeled with the amount of current flowing downstream of that particular contour. A significant fraction of the total arc current is seen to flow in the region exterior to the discharge chamber; indeed, nearly 50% of the total arc current billows far downstream in the exhaust plume before returning and attaching on the outer surface of the anode barrel. This current density pattern is consistent with the moderate magnetic Reynolds number, O(1-10), associated with the discharge flow.

For small distances over which the gradients in electron temperature, flow velocity, and collision frequencies are negligible, the electric field in the plasma may be evaluated from the difference in local floating potential measured with

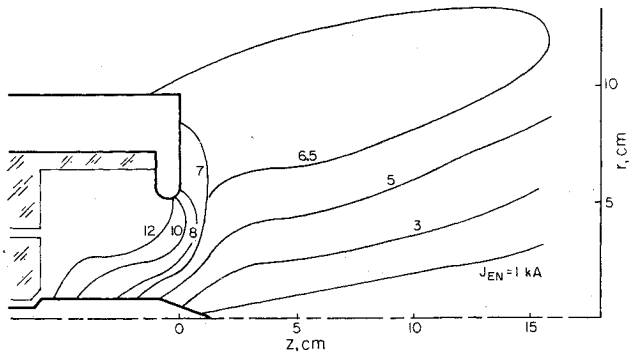

Fig. 11 Enclosed current contours: $J = 15.3$ kA, $\dot{m} = 6$ g/sec (50:50).

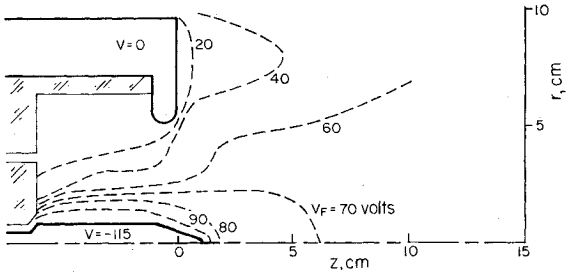

Fig. 12 Floating potential contours: $J = 15.3$ kA, $\dot{m} = 6$ g/sec (50:50).

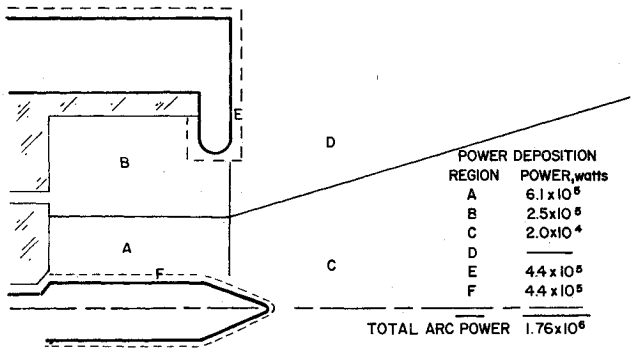

Fig. 13 $j \cdot E$ power distribution.

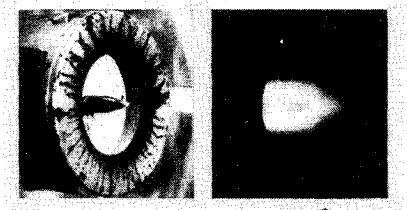

Fig. 14 Discharge luminosity.

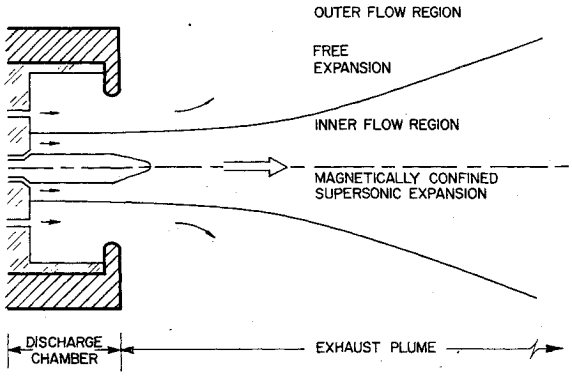

Fig. 15 Two-flow acceleration model.

simple electric probes. The distribution of equipotential contours obtained in this way is shown in Fig. 12.

Figure 13 indicates six principal regions of power deposition, and lists the total power deposited in each, as derived from the current and potential profiles. The discharge is seen to invest approximately 50% of the total arc power in the interelectrode plasma flow, while the remaining 50% appears in the electrode fall regions of the discharge. The bulk of the power addition to the plasma flow occurs within the discharge chamber, with very little power addition ensuing in the downstream exhaust, despite the large portion of arc current that flows there. This superficial paradox is a consequence of the nearly perpendicular arrangement of the current and electric field vectors in the exhaust, leading to a small value of the scalar product $j \cdot E$. However, the current in this region of the exhaust does serve a very important function in channeling the flow, as we shall see.

A closer examination of the local power deposition within the discharge chamber suggests that the two propellant flows entering via the inner and outer injection orifices become fully ionized at different axial locations inside the chamber. Enough energy is deposited adjacent to the cathode base to ionize completely the inner mass flow shortly after it enters the chamber, whereas complete ionization of the outer propellant flow is not achieved until the vicinity of the anode orifice. This model agrees qualitatively with discharge luminosity patterns, a typical one of which is shown in Fig. 14, and with spectroscopic evidence of AI present only in the outer radial regions of the discharge chamber.[21] Because of the low degree of ionization and the weak $j \times B$ forces prevailing at large radii within the discharge chamber, injected outer propellant flow is not significantly deflected inward during its passage through the chamber. This condition, the pattern of power deposition displayed in Fig. 13, and the luminosity patterns observed within the chamber, all suggest that the initial mass flow division between inner and outer propellant streams is essentially maintained as the two flows are accelerated axially downstream out of the chamber and into the exhaust regions. The plasma acceleration process may thus be conceptually treated in terms of two separate inner and outer propellant flows, schematically illustrated in Fig. 15. The actual radial demarcation between these flows, used for the flow calculations which follow, was taken to be the edge of the luminosity pattern illustrated in Fig. 14b.

The inner propellant flow is ionized, heated, and accelerated through a sonic surface within the discharge chamber. These processes may be examined in terms of a power balance wherein the flow power is partitioned between enthalpic and kinetic modes. The velocity with which the inner flow leaves the chamber thus may be expressed in terms of the local input power P_T, reduced by the radiative losses P_R, in the form

$$u_e = \left\{ 2[(P_T - P_R)/\dot{m} + 5/2R(T_e - T_i) - \int_0^{T_e} c_p(p,T)\,dT] \right\}^{1/2} \tag{7}$$

where the last two terms comprise a quasi-equilibrium expression for the flow enthalpy in terms of electron and ion temperatures, argon gas constant, and heat capacity per unit mass.[15] To evaluate this velocity, use is made of the measured input power, electron temperatures from electric probe data, static pressure measurements in the discharge chamber, and argon ion temperatures extrapolated from Doppler width data. Given the uncertainties in these numbers, the computed velocity is found to lie between 8.0 and 10.4 km/sec, which agrees well with the directly measured value of 9.6 ± 0.4 km/sec.

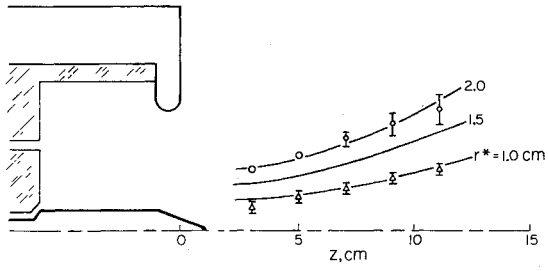

Fig. 16 Calculated and experimental mass streamlines.

After leaving the chamber, the inner flow of the discharge accelerates in the exhaust plume to a final velocity of 12.5 km/sec. This acceleration occurs over a region several anode orifice diameters long where a significant fraction of the arc current passes, as discussed earlier. Flow direction measurements within this region indicate that the mass streamlines are parallel to the local current streamlines. Hence, the electromagnetic body forces associated with the current pattern act to confine rather than to accelerate the flow. The lack of any significant radial variation in velocity justifies a 1-D approximation in describing this nozzle-like flow expansion process. Assumption of negligible recombination, along with the observed negligible energy addition during the flow expansion make the integration of the 1-D mass, momentum, and energy conservation equations straightforward. These may then be rearranged to define the mass streamlines associated with a given axial velocity profile

$$r(z) = r_0 \left[\frac{K - u_0^2/2}{K - u(z)^2/2} \right]^{1/4} [u_0/u(z)]^{1/2} \tag{8}$$

where the integration constant K represents the total specific flow enthalpy exclusive of excitation and ionization energies, and the subscript 0 implies sonic conditions. Substitution of the experimental velocity profile (Fig. 10) into Eq. (8) yields calculated streamlines in excellent agreement with the measured flow directions as illustrated in Fig. 16. The sensitivity of these results to the shape of the measured velocity profile and to the assumption of negligible recombination in the expanding flow may be examined by repeating the calculations for arbitrarily chosen velocity profiles and for arbitrary amounts of recombination enthalpy introduced into the flow equations. In all these cases, the calculated streamlines bear little resemblence to the measured flow patterns. Thus, it appears that axial acceleration in the inner exhaust plume may be adequately represented by this simple quasi one-dimensional expansion of the electromagnetically confined inner plasma flow.

Similar calculations may be repeated for the outer flow regions of Fig. 15. The lower levels of power addition yield chamber exit velocities, a factor of two less than the inner flow velocity at a similar axial location. The mass streamlines measured in the outer exhaust plume flow of the accelerator do not parallel the local current streamlines; the more rapid radical divergence of the outer exhaust flow indicates only partial electromagnetic confinement by the smaller magnetic forces there. The expansion process in this region of the discharge therefore more closely resembles that of a free expansion from a sonic orifice.

Specific Impulse of the MPD Discharge Flow

To evaluate the specific impulse associated with this flow pattern, the thrust must be calculated. Despite the simplifying assumptions of the Malliaris model,[9] an MPD arc operated at these conditions has a significant electrothermal thrust component in addition to the electromagnetic component of Eq. (1). The electrothermal contribution derives from expansion of the resistively heated discharge plasma, and may be estimated from the previously measured electron number density and electron and ion temperatures.[15] When these calculations are carried through for the $J = 15.3$ kA, $\dot{m} = 6$ g/sec case, the values in Table 1 are found for the thrust components, exhaust velocities and specific impulses.[15]

Table 1 Performance calculations

	Inner flow	Outer flow	Combined flow
Electromagnetic thrust (N)	28.0	16.0	44.0
Electrothermal thrust (N)	9.5	2.7	12.2
Total thrust (N)	37.5	18.7	56.2
$T/\dot{m}$, mass average exhaust velocity (km/sec)	12.5	6.2	9.4
$T/\dot{m}g$, specific impulse (sec)	1280	640	960

Comparison of the mass-averaged exhaust velocities with the velocities at the anode orifice suggests that approximately 30% of the arcjet's thrust is recovered during the flow expansion in the electromagnetically confined exhaust plume of the discharge. The inner flow region generates thrust with a specific impulse which considerably exceeds the "limiting" I_s of 890 sec for argon. In contrast, the outer flow produces thrust with a low specific impulse, and thus degrades the overall performance of the thruster, even though the overall specific impulse still somewhat exceeds the minimum flow power model's limit of 890 sec.

It is tempting to consider elimination or reduction of the outer flow region to increase the thruster's specific impulse further. We have seen, however, that some portion of the total propellant flow rate must be invested in the outer flow regions to maintain a minimum terminal arc voltage for a given current. Attempts to eliminate the outer flow region by reducing the anode orifice may simply produce another inner/outer flow structure in the reduced discharge volume to satisfy current continuity and charge carrier requirements. Clearly, the function and significance of the outer flow region in the MPD discharge warrant further attention.

Summary

The experiments reported here seem to countervene, at least to some degree, previous contentions of basic limitations on MPD performance. The onset of terminal voltage fluctuations has been shown not to define a unique limiting value for the $J^2/\dot{m}$ parameter, but appears to be associated primarily with cathode phenomena rather than with the interelectrode flow processes. Arcs with improved insulators, electrodes, and gas injection geometries, have been designed and operated at a specific impulse somewhat beyond the "critical" value, and the significant processes of thrust production in such arcs have been identified. The inner portions of these arc flows achieve much higher speeds and conversion efficiencies than the outer portions, suggesting that further performance improvement may be realized if the extent and influence of the outer regions can be reduced.

References

[1] Malliaris, A. C. John, R. R. Garrison, R. L., and Libby, D. R., "Performance of Quasi-Steady MPD Thrusters at High Powers," *AIAA Journal*, Vol. 10, Feb. 1972, pp. 121-122.

[2] Hügel, H., "Flow Rate Limitations in the Self-Field Accelerator," AIAA paper 73-1094, 1973, Lake Tahoe, Nev.; Also *AIAA Journal*, Vol. 12, Nov. 1974, pp. 1461-1462.

[3] Stratton, T. F., "High Current Steady-State Coaxial Plasma Accelerators," *AIAA Journal*, Vol. 3, Oct. 1965, pp. 1961-1963.

[4]Ducati, A. C., "Recent Progress in High Specific Impulse Thermoionic Acceleration," AIAA Paper 65-66, 1965.

[5]Hoell, J. M., Jr., Burlock, J., and Jarrett, O. Jr., "Velocity and Thrust Measurements in a Quasi-Steady Magnetoplasmadynamic Thruster," AIAA Paper 70-1080, 1970, Stanford, Calif.; also, *AIAA Journal*, Vol. 9, Oct. 1971, pp. 1969-1974.

[6]Cann, G. L. and Harder, R. L., "Thruster Efficiencies of Electromagnetic Engines," *AIAA Journal*, Vol. 6, March 1968, pp. 558-560.

[7]Jahn, R. G., *Physics of Electric Propulsion*, McGraw Hill, New York, 1968.

[8]Saber, A. J. and Jahn, R. G., "Anode Power Deposition in Quasi-Steady MPD Arcs," AIAA Paper 73-1091, 1973, Lake Tahoe, Nev.

[9]Malliaris, A. C., John, R. R., Garrison, R. L., and Libby, D. R., "Quasi-Steady MPD Propulsion at High Power," Final Tech. Rept. AVSD-0146-71-44, NASA CR 111872, Feb. 1971.

[10]Di Capua, M. S. and Jahn, R. G., "Energy Deposition in Parallel-Plate Plasma Accelerators," NASA 31-001-005, Aerospace and Mechanical Sciences Rept. 1015, Princeton Univ., Princeton, N. J., Dec. 1971.

[11]Clark, K. E. and Jahn, R. G., "Quasi-Steady Plasma Acceleration," *AIAA Journal*, Vol. 8, Feb. 1970, pp. 216-221.

[12]Bruckner, A. P. and Jahn, R. G., "Exhaust Plume Structure in a Quasi-Steady MPD Accelerator," *AIAA Journal*, Vol. 12, Sept. 1974, pp. 1198-1203.

[13]Boyle, M. J. and Jahn, R. G., "Power Deposition in Quasi-Steady MPD Arcs," AIAA paper 73-1090, 1973, Lake Tahoe, Nev.

[14]Hügel, H., "Self-Magnetic Effect in Arcjet Engines," *AIAA Journal*, Vol. 6, Aug. 1968, pp. 1573-1575.

[15]Boyle, M. J., "Acceleration Processes in the Quasi-Steady Magnetoplasmadynamic Discharge," Ph.D. thesis, Aerospace and Mechanical Sciences, Princeton Univ., Princeton, N. J., Oct. 1974.

[16]Ducati, A. C. and Jahn, R. G., "Investigation of Pulsed Quasi-Steady MPD Arcjets," Plasmadyne, Santa Ana, Calif., Rept. FR-061-10140, June 1971.

[17]Jahn, R. G., Clark, K. E., Oberth, R. C. and Turchi, P. J., "Acceleration Patterns in Quasi-Steady MPD Arcs," *AIAA Journal*, Vol. 9, Jan. 1971, pp. 167-172.

[18]Malliaris, A. C. and Libby, D. R., "Velocities of Neutral and Ionic Species in an MPD Flow," AIAA Paper 69-109, N.Y., Jan. 1969.

[19]Jahn, R. G., et al., "Pulsed Electromagnetic Gas Acceleration," NASA NGL 31-001-005, Aerospace and Mechanical Sciences Rept. 634w, Princeton Univ., Princeton, N. J., July 1974.

[20]Oberth, R. C. and Jahn, R. G., "Anode Phenomena in High Current Accelerators," *AIAA Journal*, Vol. 10, Jan. 1972, pp. 86-92.

[21]Jahn, R. G. et al., "Pulsed Electromagnetic Gas Acceleration," NASA NGL 31-001-005, Aerospace and Mechanical Sciences Rept. 634t, Princeton Univ., Princeton, N. J., Jan. 1973.